Nonlinear interaction of propagating short pulses in optically dense media

Opher Kinrot and Yehiam Prior
Department of Chemical Physics, Weizmann Institute of Science, Rehovot 76 100, Israel
(Received 22 December 1994)

The optical density of a resonant medium significantly affects the output signal in time resolved nonlinear optical interactions. The resonant interaction with a medium reshapes any propagating short pulse, and the mutual interaction of several such pulses, as in four-wave mixing, must be treated self-consistently. We present a theoretical framework for the proper handling of the propagation of all pulses, input as well as generated, in the small area limit. For optically thick resonant absorbers, negative time delay signals are observed, and the apparent decay rate of the induced polarization is faster than the rate observed for thin samples. We experimentally measure degenerate four-wave mixing in an atomic medium as an example, and demonstrate the quality of the theoretical model by the excellent fit to measured signals over several orders of magnitude. The improved understanding enables us to provide a simple, but surprisingly accurate, estimate for the apparent decay rate in homogeneously broadened optically thick media: If the absorption is given by α, the propagation length is L, and the transverse relaxation time is T_2, the apparent decay rate $2/T_a$ of a time resolved four-wave mixing signal is given by $2/T_a = (2/T_2)(1 + \alpha L/2)$.

PACS number(s): 42.65.Re, 42.65.Hw, 78.47.+p

I. INTRODUCTION

Nonlinear optical interactions of short pulses, such as pump-probe spectroscopy and four-wave mixing (FWM), are an important tool for the experimental investigation of excited state dynamics and for the determination of relaxation rates. They are used routinely in a wide range of research fields, from solid state physics to gas phase chemistry [1]. The common interpretation of measurements involves solving for the material response under the assumption of an optically thin sample. The theoretical analysis usually treats the nonlinear interaction perturbatively, where the third-order induced polarization includes contributions determined by the timing of the incident pulses and by phase matching considerations [2]. The transient theory is a natural extension of the perturbation treatment for cw light established many years ago by Bloembergen [3].

Since nonlinear optical processes may have large resonance enhancements, many experiments are performed under near-resonance conditions, mostly one-photon resonance, where the absorption might be non-negligible. With short pulses, the spectral width of the resonance line may be much narrower than the laser pulse spectrum and the pulses can therefore propagate many absorption lengths into the sample with only a minor loss of total energy, in apparent contradiction to Beer's law. The effect of the resonant absorption and dispersion is to modify the pulse shape, converting the pulse envelope into an oscillatory (Bessel-like) function of time. This phenomenon was first described by Crisp [4] and is sometimes described as "anomalous" classical absorption [5]. Observation of the "absorption notch" induced by propagation was reported by Friedman *et al.* [6] for nanosecond pulses and the formation of "zero area" picosecond pulses was observed by Rothenberg, Grischkowsky, and Balant [7]. Recently, propagation effects on the femtosecond time scale were rediscovered in the context of solid state physics [8] and Laenen and Laubrereau [9] and Aaviksoo *et al.* [10] used the pulse reshaping associated with absorption to estimate material dephasing times in homogeneously and inhomogeneously broadened spectral lines.

The basic nonlinear optical experiment involves an ensemble of homogeneously broadened two-level systems characterized by a polarization dephasing time T_2, which interacts with two identical short laser pulses having a time delay τ between them. For time resolved degenerate FWM, according to the "standard model" derived by Yajima and Taira [11], the FWM signal evolves as follows: the signal is zero for "negative" time delays (the "probe" pulse arrives before the "pump" pulse), increases with the pulse rise time near zero time delay, and falls exponentially for "positive" delays with a decay rate $2/T_2$. This classical analysis has been used often to derive the relaxation rates in various experimental situations, but it does not include any consideration of the effect of pulse propagation in the sample. The realization that transient FWM response may, under some circumstances, differ from the standard shape has developed as a result of experiments performed on solid state samples. Dörnfeld and Hvam [12] have observed negative time delay response in CdSe and attributed it to biexciton effects. The experimental observation of negative time delay response in FWM in GaAs quantum wells was reported by Leo *et al.* [13] and explained by Wegener *et al.* in terms of higher-order susceptibilities interfering with the third-order FWM process [14]. Polariton propagation was shown to result in oscillations of the FWM signal and observation of negative delay response in $In_xGa_{1-x}As$ quantum wells [15] and CdSe [16]. Various theoretical calculations of FWM in optically thick samples predict the appearance of negative time delay response, signal decay rates faster than the thin sample

limit, and oscillations in the FWM signal. The calculations by Belov *et al.* [17] were limited to samples whose physical length is small compared to the spatial extent of the optical pulse ($L < ct_p$), while Rappen *et al.* [18] concentrated on polaritons and Schillak and Balslev [19] on excitonic resonances.

Each of the individual experiments described above was explained within its own context, but there seems to be no general physical picture emerging to describe the influence of propagation on nonlinear interactions. Recently, we have presented experimental results and discussed an outline for a theory of four-wave mixing in an optically dense atomic medium [20]. The present work details and extends the theory, providing an intuitive and universal framework, relevant to the analysis of FWM in particular and to other nonlinear processes involving short pulses in general. We present a self-consistent model that incorporates propagation phenomena into the analysis of nonlinear interactions and allows interpretation of measurements even for strongly absorbing samples. The theory is valid for all cases where the perturbative description of the nonlinear interaction is justified and breaks down when saturation effects become important, which is the same limit where the standard perturbation series expansion for nonlinear interactions diverges. The paper includes a theoretical discussion as well as experimental results of transient FWM in a resonant atomic medium, showing excellent agreement over several orders of magnitude of signal levels and without any free fitting parameters.

Accounting for propagation effects in nonlinear optical interactions necessitates solving the coupled Maxwell-Bloch equations. We decouple the nonlinear interaction and the propagation by assuming small area pulses, i.e., the changes to the ground state population are negligible. We are thus able to solve for the propagation of each incident pulse independently, using the formalism developed by Crisp [4]. The propagated pulse envelopes (and not the incident pulses) are used in calculating the induced nonlinear polarization. The nonlinear interaction is treated perturbatively as in Yajima and Taira's [11] analysis. Emitted fields generated by the interaction are also correctly propagated through the sample to yield the observed FWM signal. The dependence of the generated FWM signal on the time delay between pulses reflects the interaction of the "self-consistent" pulse envelopes and not of the incident pulses and it is shown that the optical density of the medium affects the measurement both quantitatively and qualitatively. Even for moderate absorption, the straightforward interpretation of FWM signal decay rates as the dephasing rates of the medium gives erroneous results and the effects of propagation have to be explicitly taken into account for proper interpretation.

The outline of the paper is as follows. In Sec. II we present the general theoretical framework for the solution of both the propagation and the nonlinear interaction. The analysis introduces all the relevant pulse and material parameters and gives the most general solution for two-level systems. We further show how the results for the propagated pulse envelopes are incorporated into the calculation of induced polarizations and emitted fields. Section III deals with the impulsive limit of pulse envelopes, where we develop an analytical result for the case of small absorption and show the qualitative behavior in the strong absorption limit. In Sec. IV we discuss the manner by which calculations based on the present theory can be implemented and show the results of such calculations both for the propagation of fields and for FWM signals. Experimental results of FWM in potassium vapor are in Sec. V. We show how a "generic" picture of the measurements may be developed and analyze the good fit of the experiments to the theory. Section VI summarizes the main points of the article and provides indications as to when the propagation effects are expected to influence the measured FWM signals.

II. GENERAL TWO-PULSE INTERACTION

A. Single-pulse propagation

Consider a collection of two-level (a, b) atoms with an atomic number density N, embedded in a homogeneous dielectric characterized by a nonresonant index of refraction n. The incident electromagnetic field is linearly polarized in the x direction and is propagating in the positive z direction:

$$E(z,t) = \mathcal{E}(z,t)\cos[\omega t - kz)], \tag{1}$$

where the slowly varying pulse envelope function is $\mathcal{E}(z,t) = |\mathcal{E}(z,t)|e^{i\phi(z,t)}$ and $k = n\omega/c$. Assume a distribution of atomic transition frequencies $g(\omega_0)$, with ω_0 being the transition frequency of a single homogeneous group of atoms, $\Delta(\equiv \omega_0 - \omega)$ is the laser detuning from resonance, and the inhomogeneous distribution function $g(\omega_0)$ obeys the normalization condition $\int_{-\infty}^{+\infty} g(\omega_0)d\omega_0 = 1$.

The rotating wave approximation is used to eliminate the fast oscillations at frequency ω and obtain the Bloch equations for the polarization density, which involve only slowly varying field envelopes and density matrix elements. For each homogeneous group the density matrix evolution is given by

$$\frac{\partial}{\partial t}\rho_{ba}(z,t,\omega_0) = \frac{-i}{\hbar}\mu_{ab}\mathcal{E}(z,t)\rho_D(z,t,\omega_0) - \left(\frac{1}{T_2} + i\Delta\right)\rho_{ba}(z,t,\omega_0). \tag{2}$$

In this density matrix notation, the off-diagonal elements are ρ_{ba}, ρ_{ba}^* and $\rho_D \equiv \rho_{aa} - \rho_{bb}$ is the population difference. All the homogeneous groups are assumed to share a single polarization dephasing time T_2. The total polarization of the medium is given by

$$\mathcal{P}(z,t) = N\mu_{ab}\int_{-\infty}^{+\infty}\rho_{ba}(z,t,\omega_0)g(\omega_0)d\omega_0. \tag{3}$$

The total induced polarization should now be used as a source term in the wave equation, which describes the

propagation of the pulse in the medium. The fully coupled Bloch-Maxwell equations are difficult to solve, but a reasonable approach is to solve them in the limit where the propagation can be decoupled from the interaction. This holds for "weak" pulses, where a passing pulse leaves most of the atoms in their ground state. The quantitative definition of pulse "weakness" is given by the pulse area, where the area of a pulse is given by the rotation angle of the Bloch vector during the interaction and is defined as

$$\theta(z) = \int_{-\infty}^{\infty} \frac{\mu_{ab}\mathcal{E}(z,t)}{\hbar} dt. \tag{4}$$

The limit of validity of the present derivation is that all fields involved in the interaction (incident or induced) have a small area at all times:

$$\left| \int_{-\infty}^{t} \frac{\mu_{ab}\mathcal{E}(z,t')}{\hbar} dt' \right| \ll 1. \tag{5}$$

This assumption is consistent with the use of the lowest-order perturbation theory to derive the nonlinear polarizations involved in a four-wave-mixing process. It amounts to neglecting any saturation effects and realizing that the ground state population is not altered by the interaction. With this assumption, insert $\rho_D(z,t) = \rho_D(z,t=0) = -1$ in Eq. (2) to obtain a linear equation for the atomic polarization density

$$\left(\frac{\partial}{\partial t} + \frac{1}{T_2} + i\Delta\right) \rho_{ba}(z,t,\omega_0) = \frac{i}{\hbar}\mu_{ab}\mathcal{E}(z,t). \tag{6}$$

The Fourier transform of Eq. (6) provides an algebraic equation for the frequency components of the polarization and field, $\hat{\rho}(z,\nu,\omega_0), \hat{\mathcal{E}}(z,\nu)$, and the solution to this equation is

$$\hat{\rho}_{ba}(z,\nu,\omega_0) = \frac{i}{\hbar}\mu_{ab}\hat{\mathcal{E}}(z,\nu)[1/T_2 + i(\Delta - \nu)]^{-1}. \tag{7}$$

To describe the propagation of a pulse incident into the medium, the slowly varying envelope approximation is used in the wave equation, neglecting higher-order derivatives and keeping only the linearized form

$$\left(\frac{\partial}{\partial z} + \frac{n}{c}\frac{\partial}{\partial t}\right) \mathcal{E}(z,t) = \frac{2\pi\omega i}{nc}\mathcal{P}(z,t). \tag{8}$$

Combining Eqs. (3), (7), and the Fourier transform of Eq. (8), a frequency domain equation describing the propagation of a single short pulse in an absorbing medium of two-level atoms is obtained:

$$\left(\frac{\partial}{\partial z} - \frac{in\nu}{c} + A(\nu)\right) \hat{\mathcal{E}}(z,\nu) = 0, \tag{9}$$

$$A(\nu) = \frac{2\pi N\mu_{ab}^2\omega}{\hbar nc} \int_{-\infty}^{+\infty} \frac{g(\omega_0)}{1/T_2 + i(\omega_0 - \omega - \nu)} d\omega_0. \tag{10}$$

Integrating this equation and making an inverse Fourier transform, the field envelope at any distance z into the sample is given by

$$\mathcal{E}(z,t) = \frac{1}{2\pi}\int_{-\infty}^{+\infty} \hat{\mathcal{E}}(z=0,\nu) \times \exp[-i\nu(t - nz/c) - A(\nu)z] d\nu. \tag{11}$$

The complex term $A(\nu)$ combines the absorption and the dispersion of the induced polarization, which together with the incident field create the displacement field in the material.

B. Nonlinear polarization

The formulation of the Bloch equations and of Maxwell's wave equation in their linearized forms is made possible by the slowly varying amplitude and the rotating wave approximations. The small-area assumption decouples the two sets of equations and results in a full solution for the envelope of a single short pulse propagating through an ensemble of two-level atoms. For the case of nonlinear processes such as four-wave mixing, in the small-area limit, all saturation effects are neglected and different fields are taken to interact (to lowest order in the perturbation) with the ground state independently of each other. Thus, for two pulses incident on the sample, the propagated field envelopes $\mathcal{E}_{1,2}(z,t)$ can be derived by solving for each pulse separately. The self-consistent pulse envelopes found in this manner serve as the driving fields in a perturbation series for the higher-order polarizations.

We treat the most common four-wave-mixing situation, where two noncollinear pulses (wave vectors $\vec{k}_1, \vec{k}_2$) interact in a medium and induce a four-wave-mixing response in the direction $2\vec{k}_2 - \vec{k}_1$. Similar treatments can be used for other types of nonlinear interaction, involving more levels, more fields, or different nonlinearities. The incident fields are assumed to be plane waves and the angle between the wave vectors is taken as small enough that the problem is one dimensional along the propagation direction. The incident pulses have a time delay τ between them and nondegenerate interaction is allowed where the carrier frequencies may differ $\omega_1 \neq \omega_2$. The propagation of each pulse is solved independently in the frequency domain and by Fourier transformation, the pulse envelopes $\mathcal{E}_{1,2}(z,t)$ [Eq. (11)] are obtained.

We derive the first-order polarization induced by each pulse by performing a perturbation expansion for the density matrix elements [11]. The polarization includes components with spatial dependence $\exp(\pm ik_{1,2}z)$ and the components of interest are

$$\rho_{ba}^{(-1,0)}(z,t,\omega_0) = \frac{i\mu_{ba}}{\hbar}\int_{-\infty}^{t} \mathcal{E}_1^*(z,t') \times \exp[(1/T_2 + i\Delta_1)(t' - t)] dt' ,$$

$$\rho_{ba}^{(0,1)}(z,t,\omega_0) = \frac{-i\mu_{ba}}{\hbar}\int_{-\infty}^{t} \mathcal{E}_2(z,t') \times \exp[(1/T_2 + i\Delta_2)(t' - t)] dt', \tag{12}$$

where $\Delta_{1,2} = \omega_0 - \omega_{1,2}$ and the superscripts on ρ_{ba} indi-

cate the spatial dependence of each contribution: $(-1,0)$ for $-\vec{k}_1$ and $(0,1)$ for $\vec{k}_2$.

The interaction of each field with the polarization induced by the other field produces a population difference grating with wave vector $\vec{k}_2 - \vec{k}_1$,

$$\rho_D^{(-1,1)}(z,t,\omega_0) = \frac{2i\mu_{ba}}{\hbar}\int_{-\infty}^{t}\{\mathcal{E}_1^*(z,t'')\rho_{ba}^{(0,1)}(z,t'',\omega_0) - \mathcal{E}_2(z,t'')\rho_{ba}^{(-1,0)}(z,t'',\omega_0)\} \times \exp[1/T_1(t''-t)]dt''. \quad (13)$$

The third-order polarization component that creates the four-wave-mixing signal in the $2\vec{k}_2 - \vec{k}_1$ direction is given by

$$\rho_{ba}^{(-1,2)}(z,t,\omega_0) = \frac{-i\mu_{ba}}{\hbar}\int_{-\infty}^{t}\mathcal{E}_2(z,t''')\rho_D^{(-1,1)}(z,t''',\omega_0) \times \exp[(1/T_2 + i\Delta_2)(t'''-t)]dt'''. \quad (14)$$

Equation (14) is similar to the expression for the third-order polarization derived by Yajima and Taira [11], with allowance for nondegenerate interaction. The difference between the two approaches is not in the form of the third-order polarization, but rather in the fields that enter the calculation: we have replaced the incident fields, with the self-consistent fields, which include the interaction of each incident field with the polarization induced by itself. This change amounts to using the displacement field **D** instead of the electric field **E** in the medium.

In order to derive an expression for the field emitted in the four-wave-mixing direction, we need to solve the linearized wave equation [Eq. (8)], with the third-order polarization as a source term. Following the procedure outlined in Sec. II A, Eq. (9) is modified to include the polarization source term

$$\left(\frac{\partial}{\partial z} - \frac{in\nu}{c} + A(\nu)\right)\hat{\mathcal{E}}_3(z,\nu) = \frac{2\pi\omega i}{nc}\hat{\mathcal{P}}^{(-1,2)}(z,\nu), \quad (15)$$

$$\hat{\mathcal{P}}^{(-1,2)}(z,\nu) = N\mu_{ab}\int_{-\infty}^{+\infty}\hat{\rho}_{ba}^{(-1,2)}(z,\nu,\omega_0)g(\omega_0)d\omega_0, \quad (16)$$

with the boundary condition $\hat{\mathcal{E}}_3(0,\nu) = 0$. The solution for the generated field at the exit plane out of the sample is

$$\hat{\mathcal{E}}_3(z=L,t) = \frac{i\omega}{nc}\int_0^L\int_{-\infty}^{+\infty}\hat{\mathcal{P}}^{(-1,2)}(z,\nu) \times \exp\left[-i\nu t - \left(\frac{i\nu}{c} - A(\nu)\right) \times (z-L)\right]d\nu dz. \quad (17)$$

The expression in Eq. (17) takes into account the propagation of the generated field through the sample, adding the contributions from different z distances with their proper phases. A slow detector measuring the output intensity will thus measure

$$S(\tau) = \int_{-\infty}^{+\infty}|\mathcal{E}_3(L,t)|^2dt \quad (18)$$

for each time delay τ between the two pulses.

III. IMPULSIVE LIMIT: RESONANT HOMOGENEOUS LINE

A. Line shape and propagation

The derivation leading to Eq. (17) is very general, without a reference to a specific resonant line shape $g(\omega_0)$ or pulse shape $\mathcal{E}(0,t)$. The results of the previous sections do not depend on the specific line shapes in any way, as long as the main assumptions and approximations hold: the rotating wave approximation, the slowly varying envelope approximation, the small-area assumption, and the existance of a single polarization dephasing time.

To determine the propagator $A(\nu)$ for a specific case, the integral given in Eq. (10) must be evaluated. For the simplest case of a single homogeneously broadened transition with an incident resonant short pulse we find $g(\omega_0) = \delta(\omega)$ and

$$A(\nu) = \frac{\alpha}{1 - iT_2\nu}\ , \quad \alpha = \frac{2\pi N\mu_{ab}^2 T_2\omega}{\hbar nc}\ . \quad (19)$$

The parameter α in Eq. (19) is the absorption coefficient for weak, resonant monochromatic light. Naturally, time resolved measurements require incident pulses with durations significantly shorter than the dynamics to be measured. In our case, the pulses need to be shorter than T_2 and correspondingly the pulse spectrum is broader than the homogeneous absorption line. We can gain a great deal of physical insight by taking the impulsive limit of δ-function pulse envelopes, having $\mu_{ab}\mathcal{E}(0,t)/\hbar = \theta(0)\delta(t)$. For on-resonance excitation of a single homogeneous line, the propagated pulses include a contribution of a first-order Bessel function [4]

$$\mu_{ab}\mathcal{E}(z,\tilde{t})/\hbar = \theta(0)\left(\delta(\tilde{t}) - e^{-\tilde{t}/T_2}U(\tilde{t})\frac{\alpha z}{T_2}\frac{2J_1(x)}{x}\right), \quad x(z,\tilde{t}) = 2(\alpha z\tilde{t}/T_2)^{1/2}\ , \quad (20)$$

where $\tilde{t} = t - nz/c$ is the retarded time, α is the absorption coefficient on resonance as defined in (19), and U is the Heaviside step function. Integration reveals that the area of the pulse decays exponentially $\theta(z) = \theta(0)\exp[-\alpha z]$, while the energy does not decay.

Since we use the linear form of the Bloch and of the wave equations, a linear systems analysis [21] can be utilized to understand the origin of this reshaping of the propagated pulse. The impulse response of the system in the time domain corresponds in the frequency domain to a notch filter centered around the atomic transition frequency. The effective "stop band" of this filter is $\alpha z/T_2$ and this width determines the fraction of energy an incident impulse will lose due to absorption. The appearance of a negative Bessel function can be understood by

making an analogy to the negative diffraction pattern produced by an opaque circle on a transparent screen. A notch filter in space creates oscillations in spatial frequency domain, similar to oscillations in the time domain produced by an absorption notch. This analogy illustrates the dependence of the oscillation period of the Bessel function on the absorption: a wide stop band leads to fast oscillations, while a narrow stop band results in slow oscillations.

B. FWM: Weak absorption

In the weak absorption limit, the exponential part in the propagated pulse envelope [Eq. (20)] decays much faster than the Bessel function. For $\alpha L \ll 1$ the $2J_1(x)/x$ term may be replaced by unity and the propagated pulse envelope is written as

$$\mu_{ab}\mathcal{E}(z,\tilde{t})/\hbar = \theta(0)\left(\delta(\tilde{t}) - e^{-\tilde{t}/T_2}U(\tilde{t})\frac{\alpha z}{T_2}\right) . \quad (21)$$

The δ-function input pulse acquires a negative exponentially decaying "tail". The amplitude of this "reshaped" negative contribution is linearly related to the absorption. Combining Eqs. (2)–(4) and assuming that the population decay rate is much smaller than the polarization decay rate ($1/T_1 \ll 1/T_2$) gives an expression for the nonlinear polarization

$$\rho^{(-1,2)}(\tilde{t},z) = 2i\left(\frac{\mu_{ab}}{\hbar}\right)^3 \exp(-\tilde{t}/T_2)\int_{-\infty}^{\tilde{t}}\int_{-\infty}^{t'}\int_{-\infty}^{t''}\mathcal{E}_2(t',z)\{\mathcal{E}_2(t'',z)\mathcal{E}_1^*(t''',z) + \mathcal{E}_1^*(t'',z)\mathcal{E}_2(t''',z)\}\exp[T_2^{-1}(t'-t''+t''')]dt'dt''dt''' . \quad (22)$$

The nonlinear polarization is calculated to first order in the absorption αz, separating the cases of positive time delay ($\tau > 0$, pulse $\mathcal{E}_1$ precedes pulse $\mathcal{E}_2$) and negative time delay:

$$\rho^{(-1,2)}(\tilde{t},z) = i\theta_2^2\theta_1 U(\tilde{t}-\tau)e^{-\tilde{t}/T_2}[1-\alpha z(\tilde{t}/T_2)] \quad (\tau > 0) ,$$

$$\rho^{(-1,2)}(\tilde{t},z) = i\theta_2^2\theta_1 U(\tilde{t})e^{2\tau/T_2}e^{-\tilde{t}/T_2}\alpha z\tilde{t}/T_2 \quad (\tau < 0) . \quad (23)$$

The field emitted in the four-wave-mixing direction is derived from the nonlinear polarization by integrating the contributions from all z sections after propagation through the rest of the sample, as given by Eq. (17). We use the exact solution derived by Crisp (Ref. [4], Appendix B) to solve for the propagation of the different terms in (23),

$$\mathcal{E}_3(L,\tilde{t}) = -\frac{N\mu_{ab}\omega}{nc}\theta_2^2\theta_1 U(\tilde{t}-\tau)e^{-\tilde{t}/T_2} \times \int_0^L J_0(x) - \frac{\alpha z\tilde{t}}{T_2}\frac{2J_1(x)}{x}dz \quad (\tau > 0) ,$$

$$\mathcal{E}_3(L,\tilde{t}) = -\frac{N\mu_{ab}\omega}{nc}\theta_2^2\theta_1 U(\tilde{t})e^{2\tau/T_2}e^{-\tilde{t}/T_2} \times \int_0^L \frac{\alpha z\tilde{t}}{T_2}\frac{2J_1(x)}{x}dz \quad (\tau < 0) , \quad (24)$$

where as before $x(z,\tilde{t}) = 2(\alpha z\tilde{t}/T_2)^{1/2}$. Under the small absorption assumption ($\alpha L \ll 1$), the Bessel functions $J_0(x), 2J_1(x)/x$ are replaced by unity. Thus the generated fields are unaltered by propagation and the resulting emitted field at the exit plane of the medium is

$$\mathcal{E}_3(L,\tilde{t}) = \mathcal{E}_3(0)U(\tilde{t}-\tau)e^{-\tilde{t}/T_2}[1-\alpha(L/2)\tilde{t}/T_2] \quad (\tau > 0) ,$$

$$\mathcal{E}_3(L,\tilde{t}) = \mathcal{E}_3(0)U(\tilde{t})e^{2\tau/T_2}e^{-\tilde{t}/T_2}\alpha L\tilde{t}/T_2 \quad (\tau < 0) . \quad (25)$$

The measurement is performed on a slow detector as a function of delay and the energy in the FWM signal is integrated for each time delay τ between the pulses,

$$S(\tau) = S(0)\left\{U(\tau)e^{-2\tau/T_2}[1-\alpha L(1/2+\tau/T_2)] + U(-\tau)e^{4\tau/T_2}(\alpha L)^2/8\right\} . \quad (26)$$

The last step in the analytic derivation is to realize that we can replace $1-\alpha L(1/2+\tau/T_2)$ by $\exp[-\alpha L(1/2+\tau/T_2)]$ and get

$$S(\tau) = S(0)\left\{U(\tau)e^{-2\tau/T_2(1+\alpha L/2)}e^{-\alpha L/2} + U(-\tau)e^{4\tau/T_2}(\alpha L)^2/8\right\} . \quad (27)$$

Equation (27) provides an analytical expression for the weak absorption limit, which can be directly compared to the "standard" result derived for zero absorption.

For positive delays the absorption causes the FWM signal to decay faster than the "no absorption" limit $2/T_2$, giving instead a rate of $2/T_2(1+\alpha L/2)$. This result can be interpreted as replacing the real dephasing time by an "apparent" dephasing time of the form

$$T_a = T_2/(1 + \alpha L/2) \ . \tag{28}$$

The other part of Eq. (27), for negative delays, is nonzero only when absorption is present and the signal increases towards zero time delay at a rate of $4/T_2$, or at twice the rate for positive delays. This different rate may be explained by the fact that only the tail of the first pulse is responsible for this negative time delay signal. The maximum of the negative delay response near (immediately before) zero time delay is also lower, reduced by a factor of $(\alpha L)^2/8$.

C. FWM: Strong absorption

The strong absorption limit shows the most dramatic deviations from the thin sample result. For strong absorption ($\alpha L \gg 1$) the envelope of the propagated pulses is determined by the Bessel function in Eq. (20). No small parameter can be defined for simplifying the calculation of the generated signal. Instead, we provide some qualitative observations and look at the results of numerical integration. The propagated pulse envelopes are given by (20) and we perform the integrals (12) to find the first-order polarization induced by each pulse

$$\rho_{ba}^{(1)} = ie^{-\tilde{t}/T_2}\theta(0)U(\tilde{t})J_0(x) \ . \tag{29}$$

In addition to the exponential decay of the induced polarization, determined by T_2, a very striking additional feature is the decay of the Bessel function itself. The first zero of the Bessel function is at $x = 2.40\ldots$, or at $\tilde{t} = 1.44T_2(\alpha z)^{-1}$. Thus, for strong absorption, the time constant for polarization decay is determined by the first zero of the Bessel function and not by the exponential decay term. Since in two-pulse four-wave mixing the field of one pulse interacts with the polarization induced by the other, the effective polarization decay will manifest itself in the decay of the four-wave-mixing signal. The oscillations of the induced polarization predicted by (29) should also be discernible in the FWM signal. For positive delay times ($\tau > 0$), the signal comes from the field $\mathcal{E}_2$ interacting with the polarization that remains after field $\mathcal{E}_1$ has passed through the sample. For each distance z, the first zero of the Bessel function term in the polarization $\rho_{ba}^{(-1,0)}$ occurs at $\tilde{t} \sim T_2/(\alpha z)$. The four-wave-mixing signal includes contributions from all z slices in the sample, attenuated and reshaped by the propagation to the exit plane. Numerical solution of the equations shows oscillations in the output FWM signal, with the first "minimum" for positive delays occurring at $\tau/T_2 \sim 4/(\alpha L)$, indicating that for strong absorption the decay of the FWM signal is governed by absorption effects and *not* by the transverse relaxation. Another feature of FWM in strongly absorbing systems is the relation between the positive and negative delay responses. In the weak absorption limit, we derived a ratio of $(\alpha L)^2/8$ between the positive and negative delay responses around zero time delay. For $\alpha L \sim 1$, this rule breaks down and the responses for negative and positive delays become almost equal. Also, for large absorption a large fraction of the energy of the propagating pulse lags behind the leading impulse, which results in a nearly symmetric shape for the FWM response at negative and positive delays.

IV. NUMERICAL RESULTS

A. Propagation

The propagation of each of the pulses is solved in the frequency domain and converted back to the time domain, as shown in Eq. (11). Unlike the analytic solution given in (20) for the propagation of an impulse in a resonant medium, for any realistic pulse envelope numerical calculations are needed. For a homogeneous line, based on the linearity of the equations, the solution for the propagation of any pulse shape is a convolution of the "impulse response" (20) with the specific pulse envelope. Thus the propagated envelope of a pulse with a duration much shorter than T_2 (for weak absorption) or $T_2/\alpha L$ (strong absorption) will be very close to the analytic result for an impulse. Using Fourier transform properties, it is also possible to generalize the results to the off-resonant case. The impulse response consists of two parts: a retarded impulse and a Bessel function term. Off-resonant excitation results in an oscillatory exponent multiplying the second term, such that the off-resonant propagated impulse becomes

$$\mu_{ab}\mathcal{E}(z,\tilde{t})/\hbar = \theta(0)\left(\delta(\tilde{t}) - e^{i\Delta\tilde{t}}e^{-\tilde{t}/T_2}U(\tilde{t})\frac{\alpha z}{T_2}\frac{2J_1(x)}{x}\right) . \tag{30}$$

As before $\tilde{t}$ stands for retarded time while $x(z,\tilde{t}) = 2(\alpha z\tilde{t}/T_2)^{1/2}$ and Δ is the detuning from resonance. At very large detunings (i.e., for any finite-bandwidth pulse) the pulse propagates unaltered since the second term in the convolution averages to zero, as it should. Note also that for strong absorption, a detuning smaller than $\alpha L/T_2$ leads to the on-resonance propagated pulse envelope.

Turning to the numerical calculation details, notice that the solution for the propagated fields in Eq. (11) is given for all times and space locations. This allows the use of a single-step fast Fourier transform on a two-dimensional (t,z) grid, without the need to actually propagate solutions in the z direction. As an illustration of the effect of pulse reshaping we show in Fig. 1 the propagation of a hyperbolic secant pulse envelope in a resonantly absorbing sample. We plot (a) the power spectrum and (b) the field amplitude vs the delay for increasing distance z into the sample. The distance is measured in units of absorption length α^{-1} and the time is scaled by T_2. The interplay between the spectral shape of the pulse and its time domain behavior is evident: as the dip in the spectrum deepens and widens, the negative tail of the pulse gets stronger and develops oscillations. The period of the oscillations shortens with increasing absorption and the total area of the pulse approaches zero.

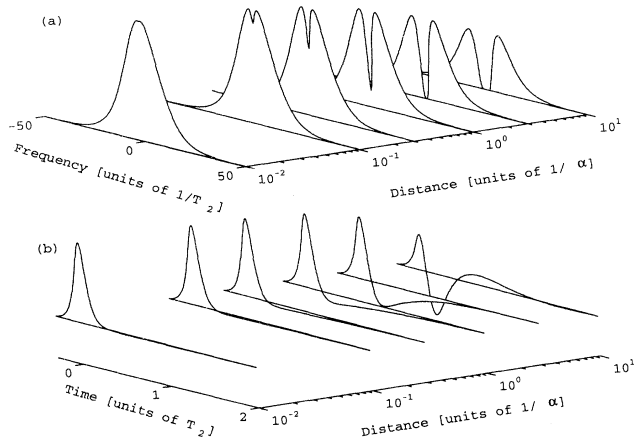

FIG. 1. Propagation of a short hyperbolic secant pulse in a homogeneously broadened medium, for $t_p/T_2 = 0.1$. (a) Power spectrum vs propagation distance in absorption lengths. Frequency is measured in T_2^{-1} units. (b) Electric field envelope $\mathcal{E}(z,t)$ vs propagation distance. Time is scaled by T_2.

B. FWM line shape

A calculation of the FWM response follows directly the procedure outlined in the previous sections. The solution for the propagated fields is calculated on a two-dimensional (t,z) grid. In a similar manner, the third-order polarization calculation is also performed on a grid, using the self-consistent fields as inputs and exchanging integration by summation. The accuracy requirements of the calculation are not very stringent: for all cases where the pulse duration is much shorter than T_2, the detailed pulse shape hardly affects the results and the grid density in time is determined only by T_2. The exact pulse shape will manifest itself at the negative side of the zero delay point at low absorption, where the FWM process resembles a cross-correlation measurement. The grid density along the propagation direction is determined by the absorption. Each z "slice" should be optically thin such that contributions along the z direction may be summed instead of integrated. The emitted FWM field is calculated in the frequency domain in order to properly account for the propagation and the FWM signal's total energy for a given delay between the pulses is found. Repeating this calculation for each time delay τ results in a plot of the calculated FWM response vs time delay between the pulses.

For an experiment where neither T_2 nor the absorption αL are known, the process of following through the whole calculation and then fitting it to the measured data might seem quite cumbersome. However, if the absorption and the dephasing time may be experimentally controlled separately, one may perform a thin sample experiment ($\alpha L \ll 1$) and T_2 can be estimated by the standard exponential fit for the positive time delay data. When this is not the case, but the pulse duration is much shorter than T_2, one can compare the measurements to a set of precalculated, "generic" plots of the impulsive FWM response for different absorption values. The absorption can be estimated from the plot with a shape (on a logarithmic scale) that best resembles the measurement and T_2 may be estimated by a time scaling that gives the best fit to the measurement. While this may not be a very rigorous method, the significant distortion of the pulse envelopes does not allow any simple extraction of the relaxation rate by observation and the procedure outlined here will result in a quick identification of the relevant parameters.

A set of generic numerical solutions of impulsive FWM for a range of absorption values is shown in Fig. 2. The ratio of pulsewidth to dephasing time is $t_p/T_2 = 0.1$ and the absorption range is $\alpha L = 0.01 - 10$. The graphs plot

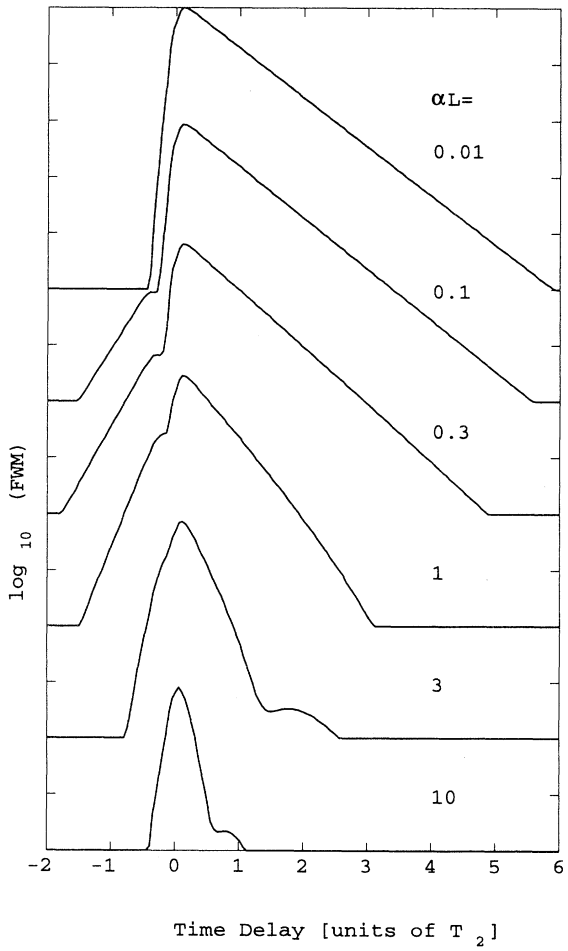

FIG. 2. Impulsive resonant FWM line shape for increasing absorption, with $t_p/T_2 = 0.1$. The absorption values are (from top to bottom) $\alpha L = 0.01, 0.1, 0.3, 1, 3, 10$. The time delay between pulses (τ) is measured in units of T_2. The vertical scale is logarithmic ($\log_{10}$) and shows five orders of magnitude of signal for each absorption value, with the graphs offset successively for clear readout.

the FWM signal over five orders of magnitude on a logarithmic scale vs scaled time delay (units of T_2). The top curve for $\alpha L = 0.01$ gives essentially the thin sample result (the Yajima-Taira case), while lower curves show the FWM signal for increasing absorption. The oscillations and fast decay in the FWM signal for large absorption are clearly seen, as well as a decrease in the peak signal amplitude. The negative delay signal increases in amplitude with increasing absorption and for low absorption has a $4/T_2$ slope as predicted from the analytical analysis. The absorption values were chosen to correspond to the normalized distances shown in Fig. 1, so the pulse envelopes and spectra given in Fig. 1 represent the pulse shape exiting the "sample" for each FWM calculation in Fig. 2.

Figure 3 shows three-dimensional views of impulsive FWM calculations, normalized in amplitude to highlight the qualitative change in line shape for increasing absorption. The top view shows mainly the positive delays while the bottom view focuses on the negative delay side. Again, a shortening of decay times as well as oscillations is clearly seen, as is the increase in the negative delay peak response with increasing absorption.

Off-resonant interaction results in less reshaping of the incident pulses and thus a closer resemblance to the thin sample predictions. In Fig. 4 we show the change in calculated FWM line shape for increasing detunings (up to one inverse pulsewidth detuning) at a constant absorption $\alpha L = 3$ (same as the fifth curve from the top in Fig. 2). The peak FWM response decreases with increasing detuning and a "coherent spike" develops.

V. EXPERIMENTAL RESULTS

A. System description

We chose to perform the experiments on an atomic vapor system, where independent variation of the absorption and of the dephasing time are carried out by controlling the temperature and the buffer gas pressure, respectively. The experiments were performed on a 2-mm cell containing potassium vapor and helium buffer gas, using the $4S_{1/2} - 4P_{3/2}$ line at 767 nm. The apparatus used was a T-shaped glass tubing structure contained inside an aluminum oven, with a spectrophotometric cell

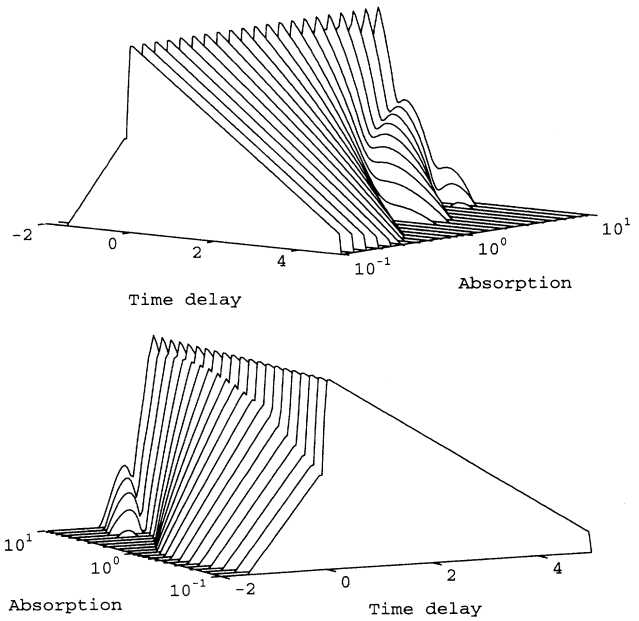

FIG. 3. Normalized impulsive FWM line shapes for increasing absorption. The vertical scale is logarithmic ($\log_{10}$) and shows five orders of magnitude, with each graph normalized to 1 at zero delay. The time delay is measured in units of T_2 and the absorption varies in the range αL=0.01 – 10. The two views show the qualitative behavior of the positive (top) and the negative delay responses. On the positive side the shortening of the decay time, as well as oscillatory behavior for high absorption, is the dominant feature. On the negative side one also notices the gradual increase of the peak response until the "step" at zero delay virtually disappears.

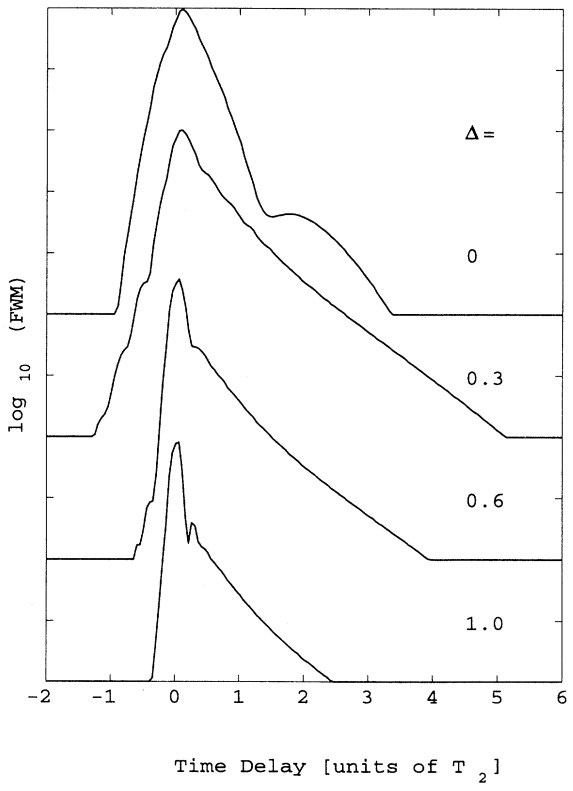

FIG. 4. Impulsive FWM line shapes for an off-resonant interaction, at absorption of $\alpha L = 3$ and $t_p/T_2 = 0.1$. FWM line shapes (on a logarithmic scale) are plotted for detunings of $\Delta = 0, 0.3, 0.6, 1$ measured in units of the FWHM of the input pulse spectrum.

(Hellma 220-QS-2) on the long horizontal arm, a cold finger containing potassium at the bottom, and a sealed valve with an outlet to a vacuum-pressure manifold on top. The temperature of the cold finger was regulated, with the rest of the oven $\sim 20°$ hotter. The laser system consisted of a hybrid mode locked double jet dye laser (Coherent 702) pumped by a frequency doubled Nd:YAG laser (Coherent Antares). The dye laser was optimized for $\sim$ 2-psec pulses with a stable spectrum and clean autocorrelation. The pulses were nearly transform limited, as was ascertained by comparing the intensity autocorrelation to the spectrum observed on an optical multichannel analyzer. The spectrum for a single pulse, when compared to that for a train of pulses, showed some spectral jitter, estimated at less than half the pulse spectral width. The pulse energy used in these experiments was $\sim$ 1 nJ/pulse, which is translated to pulse area less than 0.05 for the chosen line, so that the experiments conform to the small area assumption. We used the "folded boxcar" three-dimensional [22] phase matching geometry, where all beams propagate forward almost collinearly in the sample. All three input beams were vertically polarized and were focused into the interaction zone by a 25-cm lens. The beams were chopped at two different frequencies and the signal was detected by a phase sensitive detector at the sum frequency. Two of the beams were set for temporal coincidence while the third was variably delayed. Zero time delay was independently determined by the observation of interference fringes between any two incident beams. The inaccuracy in the zero time determination is estimated at less than ± 0.15 psec.

One major difference between the experimental conditions and the assumptions of the theoretical section is that the experiment involves a continuous measurement of the signal produced by a "train" of mode locked pulses, while the theory deals with a single "event" involving two delayed pulses. As long as the time delay between subsequent pulses in the train is large compared to the population relaxation time, $\tau_{p-p}/T_1 \gg 1$, the theoretical treatment is valid as is. Transient population grating measurements, performed under the same experimental conditions as the FWM measurements, gave an effective T_1 of 8 nsec. Since the laser operates at 76-MHz repetition rate, the pulse to pulse interval is 13.2 nsec and $\tau_{p-p}/T_1 = 1.65$. In this case, the second-order "population grating" created by the n pulse in the pulse train, $\rho_{D,n}^{(-1,1)}$, can interact with subsequent pulses $\mathcal{E}_{2,n+m}$ and the sum of all such interactions forms the third-order polarization $\rho_{ba}^{(-1,2)}$. To take this effect into account one needs to make the following replacement in Eq. (14):

$$\mathcal{E}_2(z,t''') \longrightarrow \sum_{m=0}^{\infty} \mathcal{E}_2(z,t''' - m\tau_{p-p}) e^{-m\tau_{p-p}/T_1} , \quad (31)$$

with Eq. (14) being the special case of $m = 0$. For positive delays, the only change is in the amplitude of the FWM signal and there is no change in the decay time other than for time delays very close to zero, where the two fields $\mathcal{E}_{1,2}$ overlap in time. The situation is different for negative delays. In creating a negative delay response, the propagation induced tail of the n pulse contributes to the third-order polarization, but the contribution of subsequent pulses can become larger since for the $n+1$ and later pulses the entire pulse contributes to the interaction and not only the tail. When the population decay between subsequent pulses is not rapid enough, the main contribution to the negative time delay signal comes from such interaction with population gratings that have not decayed. As a result, the FWM signal decreases (towards negative time) at a rate $2/T_2$ instead of the $4/T_2$ predicted by theory (27).

B. FWM measurements

The time resolved FWM intensity was measured at buffer gas pressures between 200 and 800 Torr, to keep the pressure broadened width larger than the Doppler width, so the resemblance to a homogeneously broadened two-level system is very good. The temperature was varied in the range 410–450 K, where for each pressure setting a set of measurements in decreasing temperatures was taken successively. For each measurement we calculate the potassium density and self-broadening from the temperature reading and published values for potassium vapor pressure and K-K collisions cross section [23]. The pressure broadening due to K-He collisions was inferred from FWM decay times at low absorption to be 0.5 cm^{-1} at a pressure of 1 atm. We thus use the temperature and buffer gas pressure readings to obtain both αL and T_2 for each measurement, which together with the measured value for T_1 and the measured autocorrelation pulse shape of the input pulses leave *no free fitting* parameters in comparing theoretical predictions

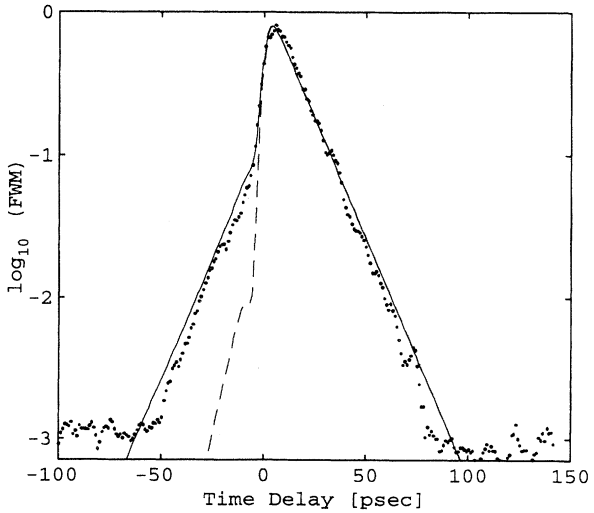

FIG. 5. Experimental FWM measurement (dots) for P=400 Torr, T=410 K, T_2=30 psec, and αL=0.3, with a calculation including the "last pulse effect" (solid line) and a calculation ignoring contributions from previous pulses (dashed line). See the text for details.

to the measured FWM signals. The theoretical calculations include the correction to Eq. (14) due to the finite pulse-to-pulse interval, i.e., using the replacement given in (31), and thus predict a $2/T_2$ slope for the negative delay response at small absorption values. For positive delays, the predicted behavior is the same as that shown in the theoretical sections.

Figure 5 shows the measured FWM signal for $\alpha L = 0.3$, with a theoretical result incorporating the replacement given in Eq. (31) (solid line) and a calculation ignoring the "last pulse effect" (dashed line). The much better agreement with the curve that includes the last pulse effect is evident.

Since the estimated T_2 is much longer than the pulse duration, the impulsive limit is valid for all the measurements. We thus find it most revealing to normalize the time in all measured results by the corresponding T_2 and get universal curves that should depend only on absorption. Figure 6 depicts a collection of such measurements, ordered from top to bottom with increasing absorption. All graphs contain FWM measurements and theoretical calculations based on the pressure and temperature readings for each one. The fit of theory and experiment over the full range of more than three orders of magnitude is excellent. At the measurements with lowest absorption (a) $\alpha L = 0.3$ and (b) $\alpha L = 0.5$, the exponential decay in both the positive and the negative delays is clear. The peak near zero time delay at (b) seems steeper because of the different time rescaling: T_2 in (a) is 30 psec and $t_p/T_2 = 0.06$, while in (b) $T_2 = 60$ psec and $t_p/T_2 = 0.03$. In (c) the absorption goes up to $\alpha L = 2.0$, while graphs (d) and (e) correspond to absorption of 2.8 and 3.3. The last two graphs (f) and (g) represent large absorption values of 5.6 and 9.6, for which

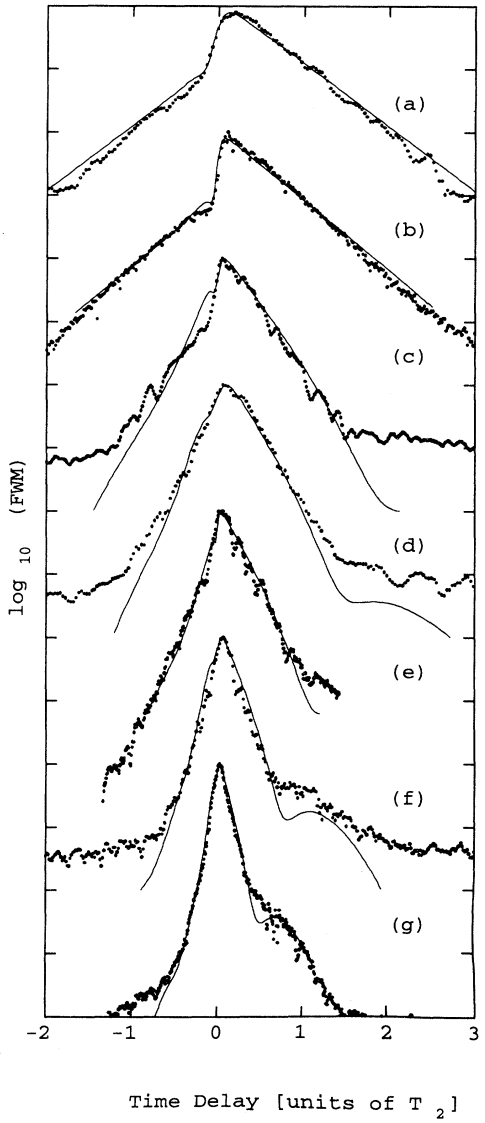

FIG. 6. Experimental measurements of $\log_{10}$ FWM signals in order of increasing absorption. The time delay for each measurement is scaled by the corresponding T_2, estimated from the temperature and pressure. Solid lines are theoretical calculations for on-resonance excitation. The pressure and temperature as well as the estimated T_2 and αL for each measurement are (a) P=800 Torr, T=410 K, T_2=30 psec, αL=0.3; (b) P=400 Torr, T=410 K, T_2=60 psec, αL=0.5; (c) P=400 Torr, T=430 K, T_2=63 psec, αL=2.0; (d) P=800 Torr, T=450 K, T_2=33 psec, αL=2.8; (e) P=200 Torr, T=410 K, T_2=126 psec, αL=3.3; (f) P=400 Torr, T=450 K, T_2=66 psec, αL=5.6; (g) P=200 Torr, T=450 K, T_2=132 psec, αL=9.6.

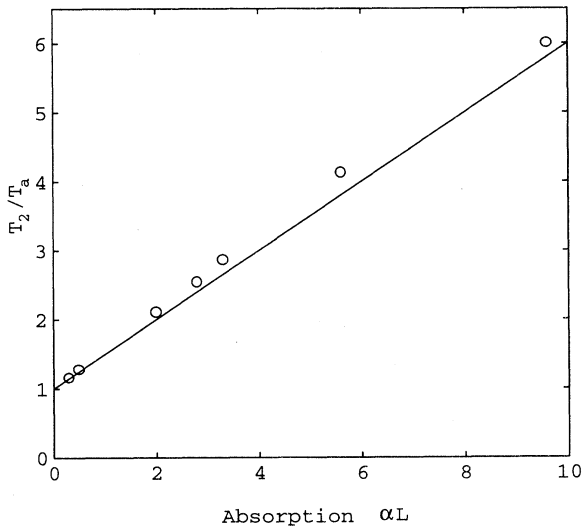

FIG. 7. Ratio between calculated dephasing times T_2 and "apparent" times T_a as a function of absorption. Values for T_2 are calculated from published collision cross sections and T_a is derived from simple exponential fits to the positive delay data in FWM measurements. The actual values for the calculated and the apparent times are (in psec): (a) 30:26, (b) 60:47, (c) 63:30, (d) 33:13, (e) 126:44, (f) 66:16, and (g) 132:22. The solid line is the analytic prediction (derived for small absorption) of $T_2/T_a = 1 + \alpha L/2$.

the FWM signal is almost symmetric around zero time delay and shows a pronounced hump for positive delays. The dips predicted by theory for positive delays at high absorption are smeared in the measurement due to off-resonant contributions. As mentioned, the pulses were almost, but not quite, transform limited and contained some pulse-to-pulse frequency jitter. The calculated dips are washed away by adding to the signal 5–10 % contribution from off-resonant irradiation detuned by a fraction of the laser linewidth. The theoretical curves in Fig. 6, however, were calculated for the on-resonance response without any additional nonresonant contributions.

It is interesting to compare the apparent decay rates $2/T_a$ (found by a simple exponential fit to the decay of the curves in Fig. 6 at positive delays) to the prediction of Eq. (28), $T_2/T_a = 1 + \alpha L/2$. The ratios between the calculated T_2 and the apparent times T_a are plotted in Fig. 7 together with the theoretical prediction. The close relation between the apparent times seen in the measurements and the theoretical predictions is carried all the way up to absorption of $\alpha L \sim 10$, even though it was derived exactly only for small absorption. It is thus possible to use this rule of thumb to extract an estimate for the real transverse relaxation time from a FWM measurement on resonance, when the absorption of the sample is known or measured separately.

VI. CONCLUSIONS

We have shown that propagation effects should be included in the analysis of any transient nonlinear measurement in optically thick media and have presented a methodology how to do it. The formalism is developed in the small area limit, valid for most experiments involving ultra short pulses interacting with a resonant transition. Moreover, the methodology presented here is not restricted to four-wave-mixing interactions. It is applicable, with the appropriate changes, to any experimental situation where short pulses nonlinearly interact with an optically thick medium. Separating the propagation from the nonlinear interaction, i.e., decoupling the Bloch and Maxwell equations, provides a physically intuitive understanding of how propagation affects the nonlinear process. The propagation induced reshaping of incident pulses is shown to manifest itself in the FWM process: the fields and the first-order polarizations acquire Bessel function envelopes, which result in steepening and oscillations in the FWM signal. An added benefit of the current analysis is the ability to use linear equations, which reduces the computational load in calculating FWM line shapes including propagation. The experimental observation of the effects predicted by the theory substantiate its validity and demonstrates its relevance to real experimental conditions.

Because the inclusion of propagation in the analysis complicates the interpretation of measurements, it is important to identify telltale signs that indicate when absorption should not be ignored. Naturally, if the weak signal peak absorption is negligible ($\alpha L < 0.1$), propagation induced effects may safely be ignored. However, when the existence of propagation effects is suspected, a cross-correlation measurement of the propagated and incident pulses can unequivocally determine the degree of pulse reshaping. In FWM experiments, negative delay response is a likely signature of propagation induced reshaping, but may also result from higher-order nonlinear processes, from a two-photon energy level, or from slow "wings" of the incident pulses. Deviation of the positive delay signal from the standard signature of a sharp (pulse limited) rise followed by a pure exponential decay and the appearance of a symmetric response around zero time delay are strong indications of substantial absorption, which in turn necessitate the use of the present formalism.

An added benefit of the present analysis is a rule of thumb for the apparent decay rate $2/T_a$. We have shown that for significant total absorption αL, the FWM signal will decay at a rate of $2/T_a = (2/T_2)(1 + \alpha L/2)$. This result, derived exactly for small absorption, is found to be approximately valid over the entire range of absorption values in the experiments [24]. Since the absorption may usually be independently determined rather simply, the determination of the apparent time T_a enables the extraction of the actual dephasing time T_2 by extrapolation to zero absorption, a very significant result.

ACKNOWLEDGMENTS

We gratefully acknowledge useful discussions with I. Sh. Averbukh, A. Szöke, and A. M. Levine. In particular, we wish to thank Professor Levine for pointing out the very useful simple expression for the apparent decay rate. The work was partially supported by the Eshkol fund of the Israel Ministry of Science and by the Minerva foundation.

[1] *Ultrashort Laser Pulses and Applications*, edited by W. Kaiser, Topics in Applied Physics Vol. 60 (Springer-Verlag, Berlin, 1988).
[2] J. G. Fujimoto and T. K. Yee, IEEE J. Quantum Electron **22**, 1215 (1986).
[3] N. Bloembergen, *Nonlinear Optics* (Benjamin, Reading, MA, 1965).
[4] M. D. Crisp, Phys. Rev. A **1**, 1604 (1970).
[5] L. Allen and J. H. Eberly, *Optical Resonance and Two-Level Atoms* (Wiley, New York, 1975).
[6] J. M. Friedman *et al.*, Opt. Commun. **20**, 183 (1977).
[7] J. E. Rothenberg, D. Grischkowsky, and A. C. Balant, Phys. Rev. Lett. **53**, 552 (1984).
[8] T. Mishina and Y. Masumoto, Phys. Rev. Lett. **71**, 2785 (1993).
[9] R. Laenen and A. Laubereau, Opt. Commun. **101**, 43

(1993).
[10] J. Aaviksoo, J. Kuhl, and K. Ploog, Phys. Rev. A **44**, R5353 (1991).
[11] T. Yajima and Y. Taira, J. Phys. Soc. Jpn. **47**, 1620 (1979).
[12] C. Dörnfeld and J. Hvam, IEEE J. Quantum Electron. **25**, 904 (1989).
[13] K. Leo *et al.*, Phys. Rev. Lett. **65**, 1340 (1990).
[14] M. Wegener, D. S. Chemla, S. Schmitt-Rink, and W. Schäfer, Phys. Rev. A **42**, 5675 (1990).
[15] T. Rappen, G. Mohs, and M. Wegener, Phys. Rev. B **47**, 9658 (1993).
[16] K. H. Pantke *et al.*, Phys. Rev. Lett. **70**, 327 (1993).
[17] M. Belov, E. Manykin, and M. Selifanov, Opt. Commun. **99**, 101 (1993).
[18] T. Rappen, G. Mohs, and M. Wegener, Phys. Status Solidi B **173**, 77 (1992).
[19] P. Shillak and I. Balslev, Phys. Rev. B **48**, 9426 (1993).
[20] O. Kinrot and Y. Prior, Phys. Rev. A **50**, R1999 (1994).
[21] A. Papoulis, *Systems and Transforms with Applications in Optics* (McGraw-Hill, New York, 1968).
[22] Y. Prior, Appl. Opt. **19**, 1741 (1980).
[23] R. B. Miles and S. E. Harris, IEEE J. Quantum Electron. **9**, 470 (1973).
[24] This behavior should be distinguished from the increase in the observed population decay time T_1 due to "radiation trapping" under similar conditions [cf. T. Holstein, Phys. Rev. **72**, 1212 (1947)]. For $T_1 \gg T_2$ and excitation by small-area pulses, as explicitly assumed in our derivation, FWM that probes excited state coherence is not affected by radiation trapping. However, the latter process might be manifested in transient grating experiments, where the FWM signal is derived from ground or excited state populations.